



## Ventilation effectiveness as an indicator of occupant exposure to particles from indoor sources

Donghyun Rim<sup>1</sup>, Atila Novoselac\*

Department of Civil, Architectural, and Environmental Engineering, The University of Texas at Austin, 1 University Station C1752, Austin, TX, USA

### ARTICLE INFO

#### Article history:

Received 23 July 2009  
Received in revised form  
22 September 2009  
Accepted 8 November 2009

#### Keywords:

Ventilation effectiveness  
Particles  
Occupant exposure  
Indoor airflow  
Source location

### ABSTRACT

Ventilation effectiveness is an indicator of the quality of supply air distribution in ventilated rooms. It is a representation of how well a considered space is ventilated compared to a perfect air mixing condition. Depending on pollutant properties and source position relative to the airflow, ventilation effectiveness can more or less successfully be used as an indicator of air quality and human exposure. This paper presents an experimentally and numerically based study that examines the relationship between ventilation effectiveness and particle concentration in typical indoor environments. The results show that the relationship varies predominantly with airflow pattern and particle properties. Fine particles (1  $\mu\text{m}$ ) follow the airflow pattern more strictly than coarse particles (7  $\mu\text{m}$ ), and the high ventilation effectiveness indicates better removal of fine particles than coarse particles. When a ventilation system provides high mixing in the space and ventilation effectiveness is close to one, particle sizes and source location have a relatively small effect on particle concentration in the breathing zone. However, when the supply air is short circuited and large stagnation zones exist within the space, the particle concentration in the breathing zone varies with particle size, source location, and airflow pattern. Generally, the results show that for fine particles (1  $\mu\text{m}$ ), increase of ventilation effectiveness reduces occupant exposure; while for coarser particles (7  $\mu\text{m}$ ), source location and airflow around the pollutant source are the major variables that affect human exposure.

Published by Elsevier Ltd.

### 1. Introduction

Providing an adequate quantity of fresh air to an occupied space is necessary for the dilution of indoor pollutant concentrations [1,2]. However, using building mechanical systems for pollutant dilution is not free. Building mechanical systems use 1/3 to 1/2 of building energy consumption, and a significant portion of this energy is used for conditioning outdoor air [3,4]. Accordingly, increase of the fresh air supply rate, as a single measure that reduces pollutant concentration, does not seem to be an adequate exposure prevention strategy.

Other ways to reduce occupant exposure to indoor airborne pollutants include controlling source emission, cleaning the air, and/or improving ventilation effectiveness. Reduction of source emission and cleaning the air are very effective ways to reduce exposure, but they necessitate the identification of each emitter or the control technology required for each type of source. These requirements are not within the scope of this study. Another alternative is to improve

ventilation effectiveness. This can be achieved by: 1) reducing poorly ventilated areas with stagnant air, 2) supplying fresh air to the occupied zones in the space, and 3) effectively removing contaminants before they spread through the space. While the supply flow rate of fresh air per unit space volume, defined as air changes per hour (ACH), represents a quantitative measure of ventilation, ventilation effectiveness is the qualitative counterpart of ventilation system performance. Ventilation effectiveness is a simple air quality indicator that can be used in both the building design phase and for on-site application. As a measure of fresh air distribution in a space, ventilation effectiveness depends on the indoor airflow pattern. Chung and Hsu [5] show that ventilation effectiveness is significantly influenced by the arrangement of inlet and outlet diffusers in the room. The study also showed little correlation between ventilation effectiveness and air exchange rate.

Ventilation effectiveness relates to both the dilution and removal of indoor airborne contaminants as it determines how efficiently supplied fresh air is distributed in the occupied space. Researchers have used several indoor air quality indicators to evaluate the effectiveness of ventilation in relation to pollution control in an occupied space [5–9]. One of the most commonly used indicators in the field is the air-change effectiveness [7,8,10]. This parameter

\* Corresponding author. Tel.: +1 512 475 8175.

E-mail addresses: [mcdhrim@gmail.com](mailto:mcdhrim@gmail.com) (D. Rim), [atila@mail.utexas.edu](mailto:atila@mail.utexas.edu) (A. Novoselac).

<sup>1</sup> Tel.: +1 512 363 8023.

describes the quality of supply air distribution in the space, based on the spatial distribution of age-of-air. Age-of-air is defined as the time elapsed from the moment that air enters the space and reaches the considered location. The local value of age-of-air in a specific location describes the freshness of air, and is directly correlated with the airflow path. Air-change effectiveness is defined as the ratio of the age-of-air for perfect mixing to the average age-of-air in a considered zone [10]. Ventilation effectiveness thus characterizes how well the occupied zone is ventilated compared with the perfect mixing condition.

However, ventilation effectiveness does not consider the pollution source position relative to the flow and occupants, and pollutant source location in an occupied space can have noticeable influences on the breathing zone concentration [11]. As a result, previous studies examined the relationship between ventilation effectiveness and occupant exposure with respect to a specific contaminant source position [6,7]. Fisk et al. [6] found a correlation between ventilation effectiveness and the removal of a passive and spatially distributed gaseous pollutant at floor level. Novoselac and Srebric [7] showed variation in the correlation between ventilation effectiveness and the concentrations of gaseous contaminants in the breathing plane for different emission source locations, i.e. occupants, floor materials, and wall paintings. A recent study by Pereira et al. [12] examined particles introduced into a space through various ventilation systems: conventional ceiling, under-floor, and split air distribution systems. The study showed that particle concentration in the breathing zone significantly varies with particle size and arrangement of inlet and outlet diffuser. Taken together, the previous studies in the literature investigated pollutant removal depending on emission source location and ventilation characteristics.

Nevertheless, the majority of previous studies analyzed gaseous types of pollutants which have different dynamics than particulate matter [5–9,11]. Particle transport in a ventilated room is governed by several factors including indoor particle source, infiltration of outdoor particles through ventilation and building envelop, filtration, deposition onto building surfaces, and particle removal by means of ventilation [13]. Particulate pollutants are as common as gaseous pollutants in occupied spaces [14], and sometimes more harmful for health [15]. Even though there have been studies on particle transport associated with indoor airflow distribution [16–21], very few explored the connection between commonly used indoor air quality indicators and the indoor particle distribution.

The aim of this study is to investigate whether ventilation effectiveness can be used as a practical air quality indicator for occupant exposure to particles from indoor sources. The study examines the correlation between the ventilation effectiveness and particle concentration considering a) the whole room and b) the occupant breathing plane, while varying the following parameters: 1) indoor airflow patterns, 2) source location, and 3) particle size. Pereira et al. [12] already analyzed the distribution of particles from various ventilation systems, and therefore this study considers particles from indoor sources.

Since the ventilation effectiveness is typically used in building designs and performance analyses for different ventilation systems, the outcome of this study should help researchers and building designers find when and how much they can rely on ventilation effectiveness as a parameter that reflects the control of particulate pollution from indoor particle sources.

The study is based on a Computational Fluid Dynamics (CFD) analysis validated with experimental measurements. The following sections present the methods used in the study and the results from the parametric analysis. The methods section includes a description of the experimental validation and applied CFD modeling methods, as well as a description of the parametric analysis. The results and

discussion section summarizes the validation results, presents the results of the parametric analysis, and discusses the overall findings of the study.

## 2. Methods

This study applied experimentally validated Computational Fluid Dynamics (CFD) methods and Lagrangian particle tracking simulations to examine airflow distribution and particle transport. Experimental measurements were conducted in a full scale environmental chamber featuring a partitioned office space. This design was chosen given that most office buildings use indoor partitions and has complex multizone airflow through open doors and between partition openings [5,17,18]. The chamber had ventilation systems with a side air supply and exhaust openings and a heated sidewall (window) which simulated typical non-isothermal boundary conditions. In this characteristic environment with supply-jet and buoyancy-driven flow tracer gas decay and particle decay tests were conducted to develop validation data. In the experiments, distributions of age-of-air and particle concentrations were measured along with other airflow parameters and boundary conditions (air speed, surface temperatures, and heat fluxes) needed for the development and testing CFD and particle tracking models. The measured data were used for the selection and adjustment of critical CFD parameters necessary for accurate airflow simulation and indoor particle transport analysis. In the subsequent phase of the study, ventilation effectiveness and particle concentrations were simulated for 54 study cases with different sources and ventilation conditions. The produced data set was used to test if the correlation between ventilation effectiveness and indoor particle concentration in the breathing plane of the room. This correlation was tested for various airflow patterns, number of air changes per hour (ACH), particle sizes, and particle source positions. The correlation data provided the basis to evaluate whether ventilation effectiveness provides information about the magnitude of exposure to indoor particles.

### 2.1. Validation of CFD and particle tracking models

Fig. 1a presents the experimental set-up for validation of the CFD and particle tracking model. The measurements were conducted in a  $5.5 \text{ m} \times 4.5 \text{ m} \times 2.7 \text{ m}$  ( $67 \text{ m}^3$ ) environmental chamber. A partition wall divided the chamber space into two zones. This partition was introduced to produce internal airflow and particle transport, and the goal was to create large gradients of age-of-air and particle concentrations in the space (Fig. 1b). To achieve this goal, the opening in the partition wall between the two zones was reduced to a smaller area than utilized in typical partitioned spaces. To lower the air mixing in the space, fresh air was supplied at  $18^\circ\text{C}$  into room air at approximately  $24^\circ\text{C}$  using a low-momentum supply diffuser (Fig. 1a). The mean velocity magnitude of the supply air at the  $0.53 \text{ m} \times 0.53 \text{ m}$  diffuser was  $0.1 \text{ m/s}$  which provided an air exchange rate of  $1.5 \text{ h}^{-1}$  and generated a vertical temperature stratification in the space. Furthermore, to generate the airflow typical in a window vicinity, the heated wall in Zone 2 of the test chamber (Fig. 1a) generated a convective heat flux of  $320 \text{ W}$ , initiating buoyancy-driven airflow near this wall. To measure the age-of-air, a tracer gas decay method was used. Particle distribution measurements were also conducted in conjunction with the decay test. These measurements of temporal and spatial particle concentration distribution in the test chamber provided sufficient data to test and adjust detailed model parameters applied in Lagrangian particle tracking models, which will be described in the CFD and Particle Tracking Simulation Parameters section.

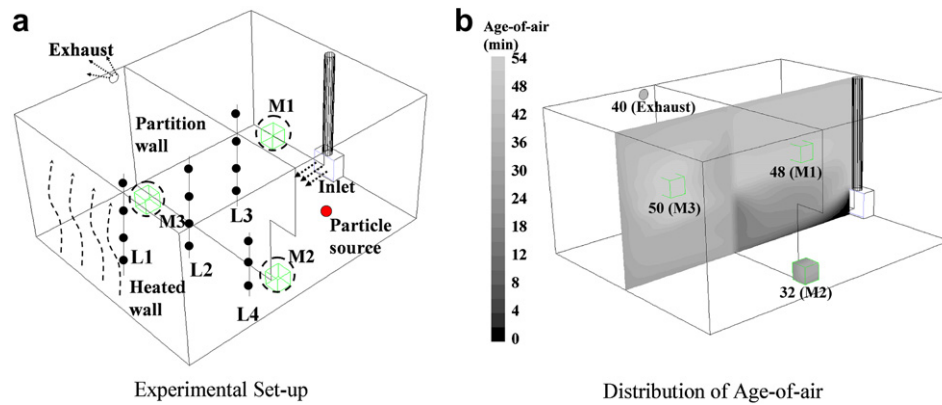


Fig. 1. Experimental set-up for CFD validation (a) and simulated distribution of age-of-air (b).

### 2.1.1. Measurement of local age-of-air and particle concentration

Airflow velocity and temperature were measured at four locations in the chamber (L1, L2, L3, and L4 in Fig. 1a). At each location, there were three to four sampling points in the vertical direction. At each sampling point, a low velocity anemometer and a temperature sensor measured air speed and temperature. Table 1 summarizes the properties and accuracies of the measurements used in the experiments.

Local age-of-air was measured by the step-down tracer gas test at the three monitoring points (points: M1, M2, and M3 in Fig. 1a) and at the exhaust. SF<sub>6</sub> tracer gas was released into the chamber at a rate of 45 L/min, and the two mixing fans dispersed the gas to both zones in the space (Fig. 1). When a uniform and sufficiently large concentration of tracer gas was achieved, the fans and tracer gas injection were terminated. After this, tracer gas decay rate was measured at the four monitoring points providing the data needed for the age-of-air calculation. Based on the measurements of the tracer gas decay, the local age-of-air at a monitoring location ( $A_i$ ) was calculated according to the ASHRAE Standard 129 [10]:

$$A_i = \Delta\tau \cdot C_{i,avg} / C_{i,start} \quad (1)$$

Where:  $\Delta\tau$  = time period of tracer gas measurements,  
 $C_{i,avg}$  = averaged tracer gas concentration at location  $i$  during  $\Delta\tau$ ,  
 $C_{i,start}$  = initial tracer gas concentration at location  $i$ .

Along with the tracer gas decay test, the particle decay was measured at the same four monitoring positions. This particle decay test provided data for the validation of particle tracking models. The test also produced data for the comparison of particle and airflow dynamics. Considering fluid and particle dynamics and air distribution in indoor environments, the small particles (particle in range of 1  $\mu\text{m}$ ) follow the air-stream more strictly than large particles (particle in range of 7  $\mu\text{m}$ ) [22]. Inertial forces and particle deposition are more significant for large particles, and therefore, validation

Table 1  
Instrumentation used in validation experiments.

Measurement	Measuring technology/ Manufacturer and model	Detection limit accuracy	Minimal logging interval
Air velocity	Omni-directional low-vel. anemometer Sensor Electronics, HT400	0.05–5 m/s	0.02 s
Temperature	Resistance (RTD)	$\pm 0.02$ m/s	30 s
	Sensor Electronics, HT400	–10–50 °C	
Tracer gas (SF <sub>6</sub> )	Electron Capture Gas Chromatograph	0.3 °C	2 min
	Lagus Applied Tech, Autotrac	0.05–5 ppb	
Coarse particles (3.2 $\mu\text{m}$ )	Optical Particle Counter	$\pm 3\%$	30 s
	TSI, Aerotrak 8220	1/m <sup>3</sup>	

cases with large particles are more challenging than validation cases with small particles [19]. However, given that concentration uniformity is much easier to achieve with small particles than with large particles, the particle decay experiment with small particles is more accurate than experiments with large particles. The particle size of 3.2  $\mu\text{m}$  was selected as a compromise between the accuracy of the validation results and the relevancy of the validation case considering the challenge for the particle tracking model.

During the test, the 3.2  $\mu\text{m}$  Latex monodisperse particles were injected by a Collison nebulizer into the space at the same location as the SF<sub>6</sub> tracer gas. Similar to the tracer gas experiment, mixing fans were used to distribute the particles uniformly. When the particle concentration in the chamber reached a significantly high level (approximately 100 times larger than background concentration), the injection and fan operation stopped, and the particle decay measurement began. Four optical particle counters (Table 1) positioned directly in the space measured the particle concentrations. These particle concentration decay results along with the tracer gas decay results were used to select the appropriate numerical simulation parameters for the CFD model (turbulence model, grid resolution, boundary conditions) and the Lagrangian particle tracking parameters (particle diffusion model, time step, number of particles, and particle deposition boundary conditions).

### 2.1.2. CFD and particle tracking simulation parameters

The experiments provided validation data as well as boundary conditions for the CFD model. Parameters for the CFD boundary conditions such as: diffuser supply velocity and turbulence intensity, surface temperature, and convective heat flux were experimentally measured in the test chamber. Airflow parameters such as air velocity, temperature, and age-of-air distribution were used for the validation of CFD results. When reasonable accuracy of the velocity field was obtained, the particle tracking model was evaluated in the following two steps. First, the CFD model sensitivity to the number of particles and time step was investigated. Second, the experimental and numerical results for different particle deposition models were compared.

All the simulations were carried out using CFD software FLUENT (2006) [23]. The Reynolds Averaged Navier-Stokes equations were used with the two equation turbulence model. Among the available two equation turbulence models, the RNG k- $\epsilon$  model was selected given its accurate prediction of turbulent indoor airflow in partitioned spaces [24]. Airflow parameters were calculated based on the Eulerian transport equations for steady-state boundary conditions. CFD grid sensitivity analysis showed that for the test chamber model a computation mesh with approximately 100,000 cells would provide a grid independent solution for temperature, velocity and

age-of-air field. Age-of-air distribution in the chamber was calculated with a method that uses a uniform tracer gas source [25]. This method uses a constant and space-uniform emission of a small amount of tracer gas into the room, and since the supply air does not contain any tracer gas, the age-of-air in the space is inversely proportional to the concentration of tracer gas [12]. The local age-of-air ( $A_i$ ) was calculated using the ratio of local concentration ( $C_i$ ), concentration at the exhaust ( $C_{\text{exh}}$ ) and the age-of-air at the exhaust which is inversely proportional to the number of air changes in the space ( $A_{\text{exh}} = 1/\text{ACH}$ ):  $A_i = C_i/(C_{\text{exh}} \cdot \text{ACH})$ .

The unsteady Lagrangian transport model was used to calculate the trajectories of particles by equating particle inertial force to external forces acting on particles including gravitational, drag, lift, Brownian, and thermophoretic force. The particle number sensitivity analysis showed that the model with a uniform initial distribution of 240,000  $3.2 \mu\text{m}$  particles in the space performed well for the 2 h particle decay analysis. The time step sensitivity analysis also showed that a time step of 0.1 s was sufficiently small for tracking the impact of turbulent airflow on particles. Given the very low volume of injected particles compared to air in the room, a one-way coupling (airflow field affects particle transport but not vice versa) was employed. The mean particle trajectory was calculated based on a time-averaged airflow field, whereas the stochastic particle trajectory due to turbulent eddies was determined by “random walk modeling”. This turbulence dispersion modeling uses a Gaussian probability distribution and a turbulence viscosity from CFD results to simulate the impact of stochastic velocity fluctuation on the particles diffusion.

When hitting a surface, particles either deposit to or rebound from the surface of impact. For particles larger than  $1 \mu\text{m}$  deposition rate is considerably different for wall and floor surfaces. In this study the deposition was considered only for the floor surfaces because for particles larger than  $1 \mu\text{m}$ , deposition velocity is 1–3 magnitudes larger on floors surfaces than on wall and ceiling surfaces [20,26]. Due to this considerably lower deposition rate of considered particles on the side wall/ceiling surfaces compared to the floor surfaces, rebound boundary conditions were used for the wall and the ceiling surfaces, while analytical data obtained by Lai and Nazaroff [26] were used for modeling of the more intensive deposition on floor surfaces. This particle deposition models did not take into account the influence of wall roughness on particle deposition, and therefore, the simulation results should be analyzed with caution as wall surface material can have significant impact on the particle deposition rate [27].

Particle deposition rate is a function of the particle size, and for the  $3.2 \mu\text{m}$  particles a previous study showed a deposition velocity of approximately 0.1 cm/s for floor surface [26]. By adjusting the threshold normal component velocity ( $V_y$ ) in the layer adjacent to the floor surface (for  $3.2 \mu\text{m}$  particle  $-V_y < 0.1 \text{ cm/s}$  rebound, or  $-V_y > 0.1 \text{ cm/s}$  deposit), the deposition velocity obtained by Lai and Nazaroff [26] was integrated in the floor deposition model.

### 2.1.3. Validation procedure

Validation of the CFD simulation was conducted by comparing the parameters from measurements with those from the simulations. For the CFD and particle tracking models, simulation parameters were selected based on measured boundary conditions, conducted sensitivity analyses, and recommendations from previous studies [28,29]. The comparison between measurements and CFD simulations included: temperature field, velocity magnitude, age-of-air distribution, and particle concentration. Temperature and velocity distributions from experiments and CFD were compared at 15 positions in the room (Fig. 1a). The simulated and measured values for age-of-air and the particle concentration were compared at the 4 monitoring locations in the space. Since the number of particles used in the

simulation was several orders of magnitude smaller than the number of particles injected during the experiment, the direct comparison was not possible. Therefore, for each monitoring point, experimental and particle tracking simulation results were compared using time-integrated particle concentrations over a period of one hour normalized by the time-integrated particle concentrations that would occur in the case of uniform particle concentration with perfect mixing in the space.

### 2.2. Simulation matrix for the study of ventilation effectiveness and particle exposure

After the validation process, the CFD and particle tracking models used in validation were modified to address a larger variety of indoor environment scenarios. Geometry parameters were changed from the validation geometry, and air supply parameters were adjusted for several typical volume flow rates and airflow distribution scenarios. Using simulation parameters that provided satisfactory accuracy in the validation case, a total of 9 airflow simulation cases were built with various geometries and airflow distribution rates (Table 2). In each case, internal heating/cooling loads were achieved by distributing convective heat loads along the object surfaces, which included human simulators, computers, floor, ceiling, and walls (Fig. 2).

For each of the cases, airflow and particle distribution were analyzed taking into account different particle properties (sizes) and source positions. Fig. 2 presents the simulated  $4 \times 6 \times 2.7 \text{ m}^3$  room geometry used in this parametric analysis. The variables controlled for the parametric analysis are as follows:

- three ventilation strategies: floor air supply, ceiling air supply, all-air heating
- three supply flow rates:  $1.93 \text{ h}^{-1}$ ,  $3.85 \text{ h}^{-1}$ ,  $7.72 \text{ h}^{-1}$
- three particle source locations: at floor, in thermal plume, close to jet
- two particle sizes:  $1 \mu\text{m}$  and  $7 \mu\text{m}$  particles

Three ventilation strategies that generate significantly different ventilation effectiveness were selected to examine typical air supply patterns found in indoor environments: low-momentum cool air supply at floor level, large momentum cool air supply close to ceiling, and hot air supply close to ceiling. The low-momentum cool air supplied at floor level (Fig. 2) generated the airflow pattern in a space where the air is moved primarily by indoor heat sources, i.e. natural convection flow. The large momentum ceiling supply (Fig. 2) produced a forced convection flow, representing a mechanically ventilated space. All-air heating was selected to represent the most common ventilation system operation that provides poor ventilation effectiveness [7]. With this system, warm air supplied at ceiling level does not often reach the lower part of the space due to the

**Table 2**  
Simulated cases for the parametric analysis.

Air Supply	Total ACH (hr <sup>-1</sup> )	Internal heating/cooling load (W)	Supply air velocity (m/s)	Supply air temperature (°C)	Supply opening area (m <sup>2</sup> )	Exhaust area (m <sup>2</sup> )
Floor air supply	1.93	500	0.088	18	0.397	0.120
	3.86	1000	0.175	18	0.397	0.120
	7.72	2000	0.35	18	0.397	0.120
Ceiling air supply	1.93	500	1.0	14	0.035	0.120
	3.86	1000	2.0	14	0.035	0.120
	7.72	2000	4.0	14	0.035	0.120
All-air heating	1.93	-400	1.0	30	0.035	0.120
	3.86	-800	2.0	30	0.035	0.120
	7.72	-1600	4.0	30	0.035	0.120

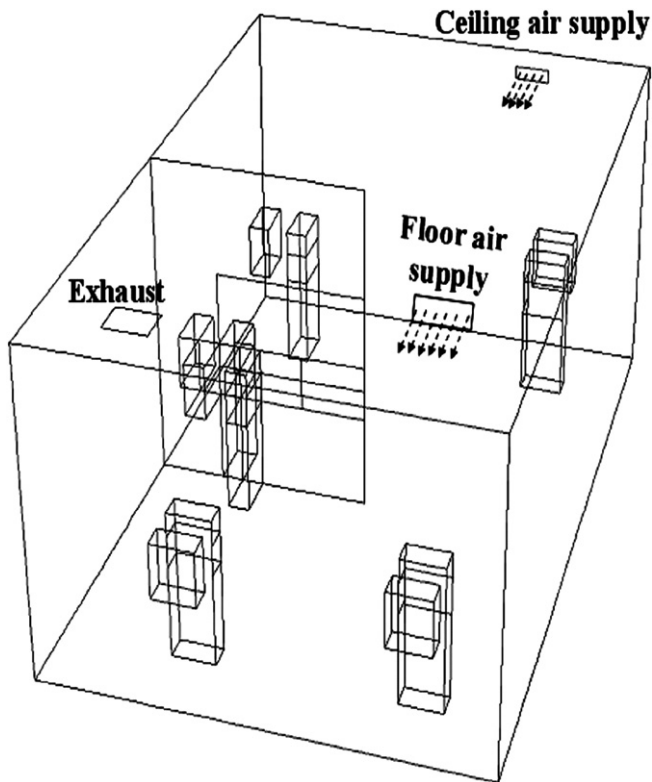


Fig. 2. Room geometry used in the CFD simulation with low-momentum floor supply, large momentum wall supply, and air heating supply.

temperature stratification. This causes short circuiting of the airflow and air stagnation in the lower part of the occupied space. The three analyzed supply flow rates were:  $1.93$ ,  $3.85$ , and  $7.72 \text{ h}^{-1}$ , and since this study considers only space particle sources, the supply flow was free of particles. Supply rates lower than  $5 \text{ h}^{-1}$  are typical of spaces in residential and moderately occupied commercial buildings [30] as well as for buildings with dedicated outdoor ventilation systems, whereas rates larger than  $5 \text{ h}^{-1}$  are common for commercial buildings with large occupancies such as buildings with cubicle office spaces. Considering these three air supply systems and three different volumes flow rates, nine airflow distributions and corresponding age-of-air distributions were calculated.

The three particle source positions were selected based on the most common particle sources encountered in the indoor environment. The injection of 240,000 particles at the source position over a short period of time simulated a realistic emission of particles due to various human activities. The first source was located on the flat surface 10 cm above the floor to simulate particles resuspended from floor surfaces by human action such as walking or vacuuming [31]. The second particle source was located 1 m above the ground in the vicinity of the heat source to mimic particle transport associated with a buoyancy-driven thermal plume such as cooking or smoking [32]. The third, so-called “momentum” source, was positioned in the breathing plane 1.1 m above the floor, simulating aerosols expelled from coughing or sneezing [33,34]. Particle transformation processes such as evaporation or nucleation were not considered, given that this study focused on the relationship between airflow pattern and particle transport.

For each source location, the transport of 1 and  $7 \mu\text{m}$  particles was simulated. The sizes of particles have a significant influence on their distribution in ventilated rooms. The  $1 \mu\text{m}$  particles are more likely to follow the airflow path, while  $7 \mu\text{m}$  particles are expected

to show more deviation from the airflow path and deposit on surfaces much faster, given their larger relaxation time [35]. Due to the coarse mesh, the calculation of a particle trajectory in the vicinity of the surfaces can be very inaccurate, and the particle tracking model in most of the cases over-predicts the particle deposition [28]. Therefore, as in the validation of the CFD model, particle deposition onto the floor surface was based on the experimental values and procedure previously described at the end of the CFD and Particle Tracking Simulation Parameters section. The overall deposition rate in the room calculated by CFD was  $0.36 \text{ h}^{-1}$  for  $1 \mu\text{m}$  particles and  $2.5 \text{ h}^{-1}$  for  $7 \mu\text{m}$  particles, which are within the ranges of deposition rate reported by Lai and Nazaroff [26].

In summary, 54 simulation cases, with 9 airflow patterns (3 ventilation strategies and 3 ventilation rates) and 6 different particle sources (3 source locations and 2 particle sizes), were used to test if ventilation effectiveness can be used as an indicator of occupant exposure to indoor particles.

### 2.3. Result presentation and particulate exposure reduction parameter

In all simulation cases the source of particles is instantaneous, emulating a sudden burst from the source. Consequently, the particle tracking modeling result presents the non-uniform temporal and spatial concentration in the space that provides information about the particle cloud distribution through the space. For each of 54 simulated cases, the normalized particle concentration (CN) was calculated as the ratio between the mean concentration of particles in a considered zone and the mean concentration in the case of perfect mixing. The mean concentration represents the average spatial values integrated over a period of 1 h. This integration time period of 1 h was selected to ensure that particle concentrations in the space decay to a level close to the concentration that existed prior to the particle burst. For a perfect mixing condition, the normalized particle concentration (CN) is equal to 1. Larger CN values ( $\text{CN} > 1$ ) indicate higher concentration in the considered space zone than the concentration with perfect mixing, and lower values ( $\text{CN} < 1$ ), lower particle concentration. This study did not consider scenarios where CN values are too high or too low due to case-specific circumstances such as a pollutant source in the vicinity of the kitchen exhaust hood ( $\text{CN} \ll 1$ ) or a pollutant source in a very stagnant zone ( $\text{CN} \gg 1$ ).

The normalized particle concentration (CN) can have values from 0 to infinity, whereas ventilation effectiveness (VE) defined by air-change efficiency ranges from 0 to 2. In addition, a larger VE value indicates better ventilation performance while CN has the opposite trend—the smaller the value, the lower the particle concentration. The discrepancy in the limit values for CN and VE and opposite trend in the scale pose difficulties in the direct comparison of CN and VE. Therefore, a novel parameter describing reduction of particles (RP) in a considered zone was developed as follows:

$$\text{RP} = \frac{2}{1 + \text{CN}} \quad (2)$$

Similar to ventilation effectiveness, RP ranges from 0 to 2, and for perfect mixing the value is equal to 1. RP values less than 1 represent a condition in which the considered zone is more polluted with a given particle source in the space than with a perfect mixing condition ( $\text{CN} > 1$ ), whereas an RP value larger than 1 indicates that the considered zone has less particles ( $\text{CN} < 1$ ) than with perfect mixing.

Ventilation effectiveness (VE) reflects the distribution of age-of-air (air freshness) in the considered space compared to the perfect mixing case, while reduction of particles (RP) indicates a relative

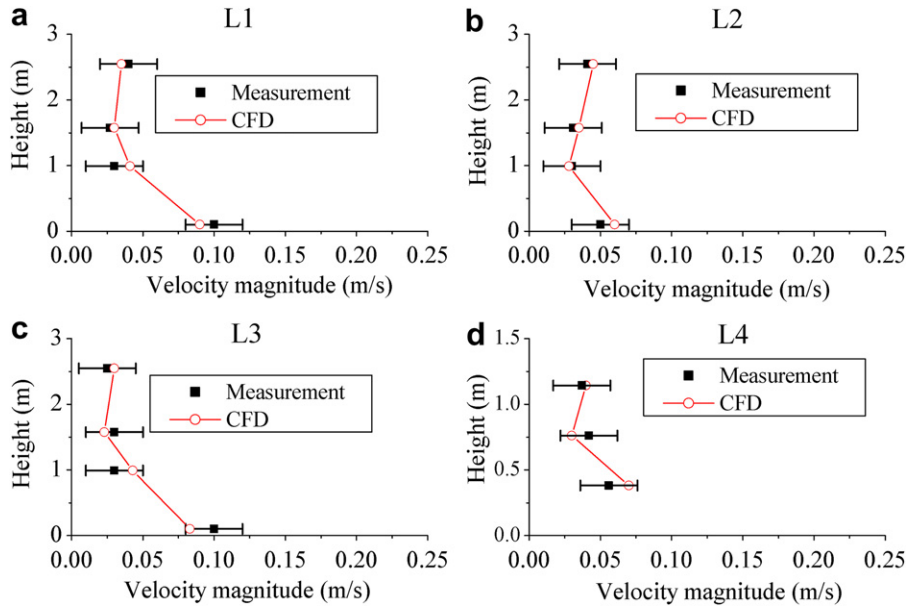


Fig. 3. CFD validation results: Velocity magnitudes at four locations (L1, L2, L3, and L4).

pollution for a given particle source. VE is only a function of airflow pattern in a space (geometry and supply air properties), while RP depends on airflow pattern, particle properties and source position. The comparison of VE and RP enables the investigation of the relationship between airflow distribution and exposure to particulate pollutants considering 1) the whole room and 2) the breathing plane of sitting occupants. The breathing plane was defined in accordance to the ASHRAE Standard 62 as the space volume (box) 0.6 m away from the chamber walls with the height ranging from 1.0 to 1.2 m above the floor (an average height of 1.1 m) [36].

### 3. Results and discussion

The study results are organized into three sections: validation of CFD and particle tracking models, major results for the parametric analysis, and applicability of ventilation effectiveness as an indicator of exposure to indoor particles.

#### 3.1. Validation of CFD simulations

Fig. 3 shows the CFD validation results comparing the velocity magnitudes from CFD simulations with those of the experimental

results. The simulated and measured velocity magnitudes ranged from 0.02 to 0.10 m/s. The simulated results agree quantitatively with the measured values to an accuracy of  $\pm 0.02$  m/s; however, some caution is needed in the interpretation of the results, especially for velocity magnitudes less than 0.05 m/s, due to the lower measurement accuracy in this velocity range. The validation results show good agreement between the simulated and measured temperature fields. Calculated and measured temperatures were compared at each of the monitoring points. The results were not graphed due to restrictions in paper length, but the results show that the difference between calculated and measured temperatures at all 15 monitoring points was below 0.6 °C.

Fig. 4 presents the distribution of age-of-air at the four monitoring positions from both the measurements and simulations. Fig. 4a indicates that the age-of-air close to the floor (M2 in Fig. 4a) is relatively small compared to the room's upper zone (M1 and M3). This trend is caused by the displacement diffuser that supplied cool air at the floor level and the upward buoyancy-driven flow that prevailed in the zone with the heated wall (Fig. 1b). Using equation (1) and the accuracy of concentration and airflow measurements, the uncertainty of age-of-air measurements is calculated to be 15%. The comparison between measured and simulated age-of-air at characteristic points shows good agreement within the uncertainty

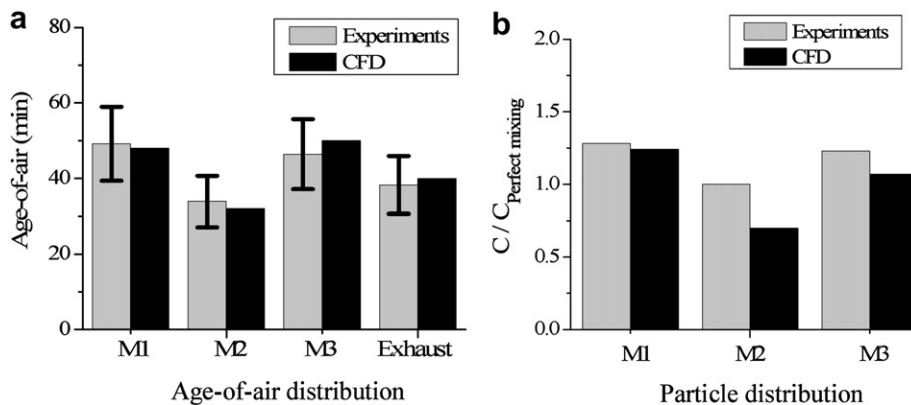


Fig. 4. Comparison of experimental measurements and simulation results for age-of-air and 3.2 μm particle distribution.

of the measurements. The results in Fig. 4a suggest that the CFD simulation is sufficiently accurate to be used in the prediction of age-of-air distribution in the partitioned indoor space.

Fig. 4b presents measured and simulated particle concentrations. The reported data are time-integrated particle concentrations for the initial 60 min of the decay test normalized with respect to a perfect mixing concentration. As described in detail in the methodology section, this normalization enables direct comparison of the measurements and simulation results on the same scale. Comparison of age-of-air and particle distribution in Fig. 4a and b (distribution for positions M1 M2 and M3) also shows that the 3.2  $\mu\text{m}$  particle concentration variation is spatially analogous to the age-of-air distribution.

Fig. 4b shows that the discrepancy in the concentration between measurement and simulation results is the largest at M2. At this point, the biggest gradients of airflow velocity and particles were observed, and even a small difference in sampling location between measurement and simulation can result in large differences. The discrepancy between experimental and simulation results at sampling point M2 could be also due to the differences in the sizes of a sampling volumes used in the experiment and the numerical model. The experimental sampling was at the very small control volume (1  $\text{cm}^3$ ), while numerical sampling used considerably larger control volume (625  $\text{cm}^3$ ). To capture the sharp gradient of the particle concentration a very small sampling control volume is needed. However, the size of the box is directly proportional to the cube of the number of particles needed to capture statistically significant number of particles in the control volume, ( $x_{\text{box}} \sim n_{\text{particle}}^3$ ), and the size of this volume was limited by the total number of simulated particles and the corresponding computational power. Since the purpose of the simulations in this study was to evaluate particle concentration in the considerably larger control volumes defined by dimensions of room (67  $\text{m}^3$ ) or breathing zone (1.5  $\text{m}^3$ ), overall validation results suggest that CFD simulation can be used to predict age-of-air and particle concentration in the space and breathing plane within reasonable accuracy.

### 3.2. Parametric analysis

Table 3 lists the basic case parameters used in the parametric analysis. The variables included the air supply pattern, air exchange rate, and heating/cooling load. The supply flow rate and the corresponding air exchange rate were determined based on heating/cooling load. The position and area of the supply opening defined the boundary conditions for the airflow simulation.

With the low-momentum air supply at floor level, the mean air speed ranged from 2.9 to 6.7  $\text{cm/s}$  for the whole room and from 1.8 to

5.4  $\text{cm/s}$  for the breathing plane. With the floor supply, the ventilation effectiveness is lower within the whole room than within the breathing plane. This trend is due to the airflow distribution characteristic for displacement ventilation, which causes low values of mean age-of-air in the breathing plane.

With the ceiling air supply and cooling regime, the air speeds are the highest among the three air supply patterns, ranging from 6.4 to 23  $\text{cm/s}$ . This relatively high air speed generates intensive air mixing and nearly uniform distribution of age-of-air in the room. This causes the VE values to be close to 1.

With all-air heating, the mean air speed ranges from 3.1 to 16  $\text{cm/s}$  for the whole room and from 1.5 to 7.9  $\text{cm/s}$  for the breathing plane. In this case, warm air supplied at the ceiling level stays in the upper part of the space, bypassing the occupied zone. This airflow pattern causes high values of age-of-air in the breathing plane. Accordingly, VE values are relatively small (0.59–0.92) compared to those associated with floor and ceiling air supply. The small VE suggests that significant short circuiting can occur with all-air heating systems.

Beside ventilation effectiveness for the cases used in this study, Table 3 shows the reference values from other studies. The ventilation effectiveness for the whole room investigated in this study are similar to those reported by Fisk et al. [6]. In their study Fisk et al. [6] measured VE values ranging from 0.69 to 0.91 in nineteen heating conditions, and VE values ranging from 0.99 to 1.15 in four cooling tests. Also, the values of ventilation effectiveness for specific flow used in this study are in the range reported by Fisk et al. [6] and Novoselac and Srebric [7]. This indicates that the selection of simulation cases represent those most typical of indoor environments.

Table 4 shows the normalized concentration (CN) of 1  $\mu\text{m}$  and 7  $\mu\text{m}$  particles for three source locations and nine different airflow patterns (three characteristic airflows and three airflow rates). For both particles, CN ranges from 0.04 to 45 for 1  $\mu\text{m}$  particles and from 0.14 to 72.6 for 7  $\mu\text{m}$  particles. The variation of CN in the breathing plane (Table 4) suggests that occupants can be exposed to a wide range of particle concentrations depending on the airflow pattern, flow rate, particle properties and source position.

When comparing the average and standard deviation of CN associated with airflow pattern, the variation is the smallest for cases with ceiling air supply ( $1.41 \pm 0.37$ ) and the largest for cases with all-air heating ( $4.5 \pm 13.8$ ). It seems that ceiling air supply leads to intense air mixing in the space, and accordingly particle concentrations similar to those with the perfect mixing condition. Conversely, all-air heating has a very small effect on air mixing and therefore the particle concentration with all-air heating varies widely depending on the source location and airflow rate. Particle concentration in the space is also relatively high with all-air heating

**Table 3**  
Simulation condition.

Air Supply	ACH ( $\text{hr}^{-1}$ )	Heating/cooling load <sup>a</sup> ( $\text{W/m}^2$ )	Mean air speed (m/s)		Ventilation effectiveness (VE)		Reference values of VE
			Whole room	Breathing plane	Whole room	Breathing plane	Whole room
Floor air supply	1.93	20.8	0.029	0.018	1.09	1.30	1.1–1.8 <sup>b</sup>
	3.86	41.7	0.041	0.030	1.07	1.00	
	7.72	83.3	0.067	0.054	1.14	1.66	
Ceiling air supply	1.93	20.8	0.064	0.064	1.03	1.03	0.9–1.1 <sup>b</sup>
	3.86	41.7	0.12	0.10	0.96	0.95	0.99–1.15 <sup>c</sup>
	7.72	–83.3	0.23	0.14	0.92	0.88	0.9–1.1 <sup>d</sup>
All-air heating	1.93	–16.7 <sup>a</sup>	0.031	0.015	0.59	0.53	0.68 <sup>b</sup>
	3.86	–33.3 <sup>a</sup>	0.068	0.037	0.78	0.73	0.69–0.91 <sup>c</sup>
	7.72	–60.7 <sup>a</sup>	0.16	0.079	0.92	0.92	

<sup>a</sup> +: cooling, -:heating.

<sup>b</sup> Data from Novoselac and Srebric [7].

<sup>c</sup> Data from in Fisk et al. [6].

<sup>d</sup> Data from Persily et al. [8].

**Table 4**  
Normalized average particle concentrations (CN): 1 μm and 7 μm.

Air supply	ACH (hr <sup>-1</sup> )	CN for 1 μm						CN for 7 μm					
		Whole room			Breathing plane			Whole room			Breathing plane		
		S1 <sup>a</sup>	S2 <sup>b</sup>	S3 <sup>c</sup>	S1	S2	S3	S1	S2	S3	S1	S2	S3
Floor air supply	1.93	1.23	1.85	1.87	1.59	0.4	0.09	1.35	3.90	2.07	1.49	2.03	16.9
	3.86	1.07	1.37	1.19	1.24	1.78	1.85	1.2	1.2	0.58	2.02	2.9	2.95
	7.72	1.12	0.38	1.32	1.41	0.04	8.25	1.19	0.83	2.69	2.00	0.36	10.94
Ceiling air supply	1.93	1.3	1.36	1.4	1.20	1.32	1.44	0.98	0.93	1.09	1.86	2.02	2.16
	3.86	1.17	1.10	1.25	1.24	1.13	2.05	1.05	1.05	1.24	1.68	1.52	2.70
	7.72	1.29	1.30	1.44	1.21	1.19	1.54	1.28	1.29	1.43	1.5	1.39	1.79
All-air heating	1.93	1.49	1.01	1.8	1.12	0.49	2.86	0.96	2	1.77	0.93	1.95	5.71
	3.86	1.24	1.19	3.35	0.74	0.82	45	0.52	1.56	1.59	0.9	1.49	72.6
	7.72	1.33	1.1	0.12	1.15	0.91	0.3	0.8	0.97	0.14	1.51	1.69	0.40

<sup>a</sup> S1: floor source.  
<sup>b</sup> S2: occupant source.  
<sup>c</sup> S3: momentum source.

compared to those with the other air supplies. For perfect mixing, CN is equal to 1. The smaller CN represents the larger reduction of particles in the space. The next section compares reduction of particles with ventilation effectiveness.

3.2.1. VE and RP values defined for the whole room

Fig. 5 illustrates the relationship between ventilation effectiveness (VE) and reduction of particles (RP) calculated based on CN for the whole room (Equation (2)). The figure illustrates the effects on three parameters: (1) airflow supply pattern, (2) air exchange rate, and (3) source location. Fig. 5a and Fig. 5b present the results for 1 μm and 7 μm, respectively. The 'x' axis refers to VE that is only a function of airflow pattern, and the 'y' axis shows values for RP, which also depends on particle position and properties. For perfect mixing, VE is equal to 1 and RP is equal to 1. The results in Fig. 5 show that VE for the whole room varies with the airflow pattern. VE values are 1.0–1.2 for floor supply (round symbols), 0.9–1.0 for ceiling supply (rectangular symbols), and 0.5–0.95 for air heating (triangular symbols).

Considering the RP for 1 μm particles defined for the whole room (Fig. 5a), ventilation with floor supply (round symbols) have larger RP values and cause smaller exposure than all-air heating (triangle symbols). With ceiling supply (square symbols) and good mixing

(VE ~ 0.95), the corresponding values of RP are in a narrow range around 0.9. This result indicates that high VE, associated with floor supply, leads to the smaller concentration of 1 μm particles in the space, whereas smaller VE, due to short circuiting, leads to a larger concentration of small (1 μm) particles in the room. Considering the effect that the position of particles sources have on RP (differentiated by symbol color), it seems that the overall concentration of small particles in the space is reduced more effectively with the source within the thermal plume than with momentum or floor sources. The results in Fig. 5a show that the change of RP with different volume flow rates (differentiated by symbol size) is relatively small. This shows that RP, as a normalized parameter that shows the quality of ventilation with respect to particle removal, has a low dependency on the airflow rate.

Fig. 5b shows the VE and RP for 7 μm particles, defined for the whole room. Compared to 1 μm particles, RP values for 7 μm particles with VE values larger than 1 (Fig. 5) are in the low range. This indicates that reduction of particles associated with high ventilation performance is generally more effective for small particles than for large particles. This is likely due to the large relaxation time of 7 μm particles compared to 1 μm particles. The results show that in most analyzed cases with a floor air supply, the retention time of 7 μm is

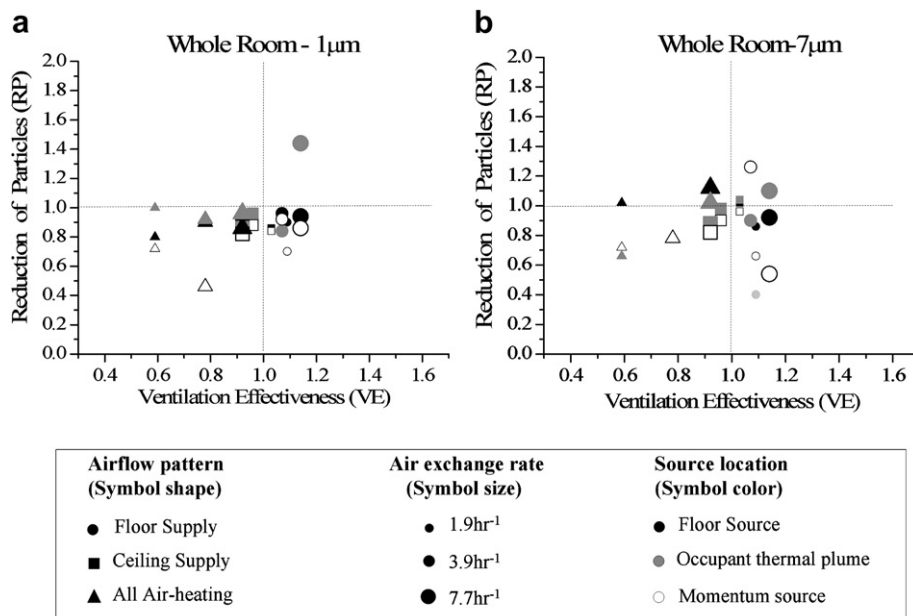


Fig. 5. Ventilation effectiveness vs. Reduction in particle concentration for whole room: (a) 1 μm and (b) 7 μm.

greater than that of the 1  $\mu\text{m}$  particles. In this case, the dominant upward buoyancy-driven flow has a smaller effect on large particles with strong gravitational forces than on small particles that are driven primarily by the air-stream. These results are in good agreement with the study by Zhao and Wu [37], which shows that for air exchange rates in the range from 2 to 8  $\text{h}^{-1}$ , 1  $\mu\text{m}$  particles likely follow the airflow path, whereas 7  $\mu\text{m}$  particles cannot be treated as a passive contaminant.

The comparison of Fig. 5a and b shows that RP values for the 7  $\mu\text{m}$  with ceiling supply ( $\text{VE} \sim 0.95$ ) are much more scattered than RP values for 1  $\mu\text{m}$  particles. This indicates that sources position of large particles have a much greater effect on the particle concentration in the space. Note that for the all-air heating cases and very low VE, RP values are small for both 7 and 1  $\mu\text{m}$  particles. This result implies that low VE is a good indicator of higher exposure to particles regardless of particle size.

### 3.2.2. VE and RP values defined for the breathing plane

Fig. 6 shows VE and RP values defined for the breathing plane of a sitting person (height ranging from 1.0 to 1.2 m above the floor). The VE values for the breathing plane are more scattered than those observed for the whole room shown in Fig. 5. The ranges of VE for the breathing plane are: 1.2–1.7 for the floor supply (round symbols), 0.9–1.0 for the ceiling supply (rectangular symbol), and 0.5–0.95 for the air heating supply (triangular symbol). The large variation of VE for the breathing plane (Fig. 6) indicates much larger effects of ventilation systems on the air freshness in the breathing plane than in the whole room. Also, ranges of RP values are much greater in the breathing plane (Fig. 6) than in the whole room (Fig. 5). The large variation in RP for the breathing plane implies that the particle concentration in the breathing plane is very sensitive to airflow pattern, particle properties and source location.

Fig. 6a shows larger RPs for 1  $\mu\text{m}$  particles with floor supply (round symbol) than with the other two air distribution systems. It seems that the floor supply system is more effective for removing 1  $\mu\text{m}$  particles in the breathing plane compared to ceiling distribution systems or air heating systems. The floor supply system generates stratified airflow where the air moves slowly from the floor to the ceiling area. This flow pattern can also explain the lower

RP values for the floor supply (dark round symbols in Fig. 6a); the floor particles are driven with the slow stratified flow. Therefore, it takes a longer time to remove the particles at floor level than those associated with momentum or thermal plume in the upper part of the room. The results with a ceiling supply (rectangular symbol in Fig. 6a) show that RP and VE values are grouped in the center of the diagram. These results indicate that with good air mixing ( $\text{VE} \sim 0.95$ ) particle concentration in the whole space and in the breathing plane are generally similar. This also means that particle source position has little effect on the increase/decrease of exposure with airflow distribution system that provides high air mixing. This result is similar to the result reported by Novoselac and Srebric [7], which indicates that with mixing airflow, the removal of gaseous pollutant does not depend on the source location. As for air heating and low VE values (Fig. 6a), it seems that there is no specific relationship between VE and RP for 1  $\mu\text{m}$  particles. With the air heating, RP ranges from 0.04 to 1.6 depending on air exchange rate and source location. This trend implies that with all-air heating, particle concentration in the breathing plane significantly varies with ventilation rate and source location.

Fig. 6b presents results for 7  $\mu\text{m}$  particles. Compared to 1  $\mu\text{m}$  particles (results in 6a), the results show generally lower ranges of RPs for 7  $\mu\text{m}$  particles. As in the whole room, the low reduction for large particles in the breathing plane seems to be caused by long residency time. The long residence time of 7  $\mu\text{m}$  particles in the breathing plane results in higher exposure than that associated with perfect mixing ( $\text{RP} < 1$ ). Also, results in Fig. 6b show that with floor and air heating supplies (cases with large and small VE, respectively), there are no specific patterns of RP value distribution. With these airflow patterns, RP varies with air exchange rate and source location and the values are scattered all around the diagram. This large variation indicates that air mixing and source positions have a much larger effects on exposure to 7  $\mu\text{m}$  particles than the ventilation effectiveness.

### 3.2.3. Applicability of ventilation effectiveness for particle exposure analyses

The ventilation effectiveness (VE) as an indicator of ventilation performance is often associated with indoor air quality and human

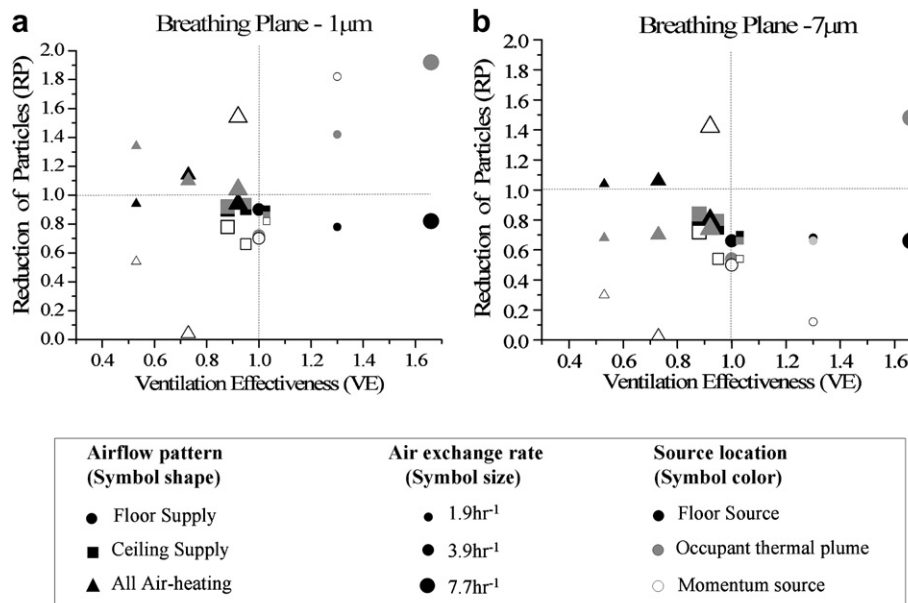


Fig. 6. Ventilation effectiveness vs. Reduction in particle concentration for breathing plane: (a) 1  $\mu\text{m}$  and (b) 7  $\mu\text{m}$ .

exposure to indoor pollutants. Since VE is only a function of airflow distribution and does not require information on source location or properties, it is a simple air quality indicator that can be used in both the building design phase and in on-site application. In this study of nine characteristic indoor airflow patterns, VE ranged from 0.5 to 1.66, with larger ranges when VE is defined for the breathing plane than for the whole room. The study results show large variations in the reduction of particle concentration (RP) values depending on airflow pattern, air exchange rate and source location. The results suggest that the particle concentration in the breathing plane is more sensitive to local airflow and source location when compared to the concentrations within the whole room space.

High values of VE and RP occur with a stratified flow, when cool air is supplied at the floor level. This trend seems to be more apparent with 1  $\mu\text{m}$  particles, but not with 7  $\mu\text{m}$  particles. With the ventilation system that provides a large mixing with the jet of cool air at the ceiling level, VE and RP values are similar to those associated with perfect mixing. In this case, the source location and particle size do not have a large influence on particle removal. With all-air heating, RP varies to a large extent with source location and particle size. In general, for cases with small VE, specific source location and airflow around pollutant source are deterministic factors for the particle removal rate.

The phenomenon common to almost all analyzed cases is that low ventilation effectiveness ( $VE < 1$ ) results in low particle exposure reduction ( $RP < 1$ ), indicating higher exposure to particulate matter than with perfect mixing. Also, the distribution of results in Figs. 5 and 6 for 1  $\mu\text{m}$  particles shows a weak correlation between VE and RP. This weak correlation does not guarantee that high ventilation performance ( $VE > 1$ ) provides high exposure reduction when compared to perfect mixing. However, it shows that in general, an increase of ventilation effectiveness results in a reduction of particulate pollutants in the space and breathing zone. This trend is apparent for 1  $\mu\text{m}$  particles, but it is not clearly identified for 7  $\mu\text{m}$  particles, likely due to their larger deviation from the air-stream.

One limitation of the present study is that the examined relationship between VE and RP is based on three representative airflow patterns but only one room size. Future studies with additional cases that analyze the effects of variation in diffuser geometry, air supply flow rate, room size, and extra particle source positions including outdoor sources introduced through the ventilation system may provide greater insight into the relationship between VE and particulate exposure. Another limitation is that this study did not consider particle transformation processes associated with ultrafine particles ( $< 100 \text{ nm}$ ) such as coagulation, evaporation or nucleation. As ultrafine particles can experience chemical transformation processes in typical indoor environments [38], future study on particle distribution in a ventilated room should consider the effects of coagulation and evaporation.

#### 4. Conclusions

Airflow distribution in an occupied space determines transport and removal of particulate pollutants. The present study examined the relationship between ventilation effectiveness and concentration of particles from indoor sources in typical indoor environments, while varying: heating/cooling load, ventilation rate, airflow pattern, particle size and source location. The results show that the relationship varies mainly with airflow pattern and particle properties. Small particles follow the airflow pattern more strictly than larger particles, and the high ventilation effectiveness indicates better removal of 1  $\mu\text{m}$  particles than 7  $\mu\text{m}$  particles. With large mixing in the space, particle removal is similar to that associated

with perfect mixing, and particle size and position have a very small impact on human exposure variation. With large air stagnation zones in the space and correspondingly low ventilation effectiveness, the exposure to both 1  $\mu\text{m}$  and 7  $\mu\text{m}$  particles is higher than with perfect mixing. In this case the concentration in the breathing zone varies to a large extent with source location and airflow pattern. Generally, the results show that for small particles an increase of ventilation effectiveness decreases occupant exposure to small particles, while for large particles source location and airflow around a pollutant source are the most important factors concerning occupant exposure.

#### References

- [1] Daisey JM, Angell WJ, Apte MG. Indoor air quality, ventilation and health symptoms in schools: an analysis of existing information. *Indoor Air* 2003;13: 53–64.
- [2] Wargocki P, Wyon DP, Sundell J, Clausen G, Fanger PO. The effects of outdoor air supply rate in an office on perceived air quality, Sick Building Syndrome (SBS) symptoms and productivity. *Indoor Air* 2000;10:222–36.
- [3] Sherman MH, Matson N. Residential ventilation and energy characteristics. *ASHRAE Transactions* 1997;103:717–30.
- [4] Emmerich SJ, Persily AK. Energy impacts of infiltration and ventilation in U.S. Office buildings using multizone airflow simulation. In: *Proceedings of IAQ and energy*, New Orleans, LA; 1998. p. 191–203.
- [5] Chung KC, Hsu SP. Effect of ventilation pattern on room air and contaminant distribution. *Building and Environment* 2001;36:989–98.
- [6] Fisk WJ, Faulkner D, Sullivan D, Bauman F. Air change effectiveness and pollutant removal efficiency during adverse mixing conditions. *Indoor Air* 1997;7:55–63.
- [7] Novoselac A, Srebric J. Comparison of air exchange efficiency and contaminant removal effectiveness as IAQ indices. *ASHRAE Transactions* 2003;109:339–49.
- [8] Persily AK, Dols WS, Naninger SJ. Air change effectiveness measurements in two modern office buildings. *Indoor Air* 1994;4(1):40–55.
- [9] Kato S, Yang JH. Study on inhaled air quality in a personal air-conditioning environment using new scales of ventilation efficiency. *Building and Environment* 2008;43:494–507.
- [10] ASHRAE. ASHRAE standard 129 – measuring air-change effectiveness. Atlanta, GA: American Society of Heating, Refrigerating and Air-Conditioning Engineers; 2004.
- [11] Kim T, Kato S, Murakami S. New scales for assessing contribution ratio of pollutant sources to indoor air quality. *Indoor and Built Environment* 2007;16:519–28.
- [12] Pereira ML, Graudenz G, Tribess A, Morawska L. Determination of particle concentration in the breathing zone for four different types of office ventilation systems. *Building and Environment* 2009;44:904–11.
- [13] Nazaroff WW. Indoor particle dynamics. *Indoor Air* 2004;14:175–83.
- [14] Wallace L. Indoor sources of ultrafine and accumulation mode particles: size distributions, size-resolved concentrations, and source strengths. *Aerosol Science and Technology* 2006;40(5):48–360.
- [15] Utell MJ, Frampton MW, Zareba W, Devlin RB, Cascio WE. Cardiovascular effects associated with air pollution: potential mechanisms and methods of testing. *Inhalation Toxicology* 2002;14:1231–47.
- [16] Abadie MO, Limam K. Numerical evaluation of the particle pollutant homogeneity and mixing time in a ventilated room. *Building and Environment* 2007;42:3848–54.
- [17] Chang TJ, Hu TS. Transport mechanisms of airborne particulate matters in partitioned indoor environment. *Building and Environment* 2008;43: 886–95.
- [18] Chung KC. Three-dimensional analysis of airflow and contaminant particle transport in a partitioned enclosure. *Building and Environment* 1999;34: 7–17.
- [19] Lai ACK, Wang K, Chen FZ. Experimental and numerical study on particle distribution in a two-zone chamber. *Atmospheric Environment* 2008;42:1717–26.
- [20] Tian ZF, Tu JY, Yeoh GH. CFD studies of indoor airflow and contaminant particle transportation. *Particulate Science and Technology* 2007;25:555–70.
- [21] Zhao B, Zhang Y, Li XT, Yang X, Huang D. Comparison of indoor aerosol particle concentration and deposition in different ventilated rooms by numerical method. *Building and Environment* 2004;39:1–8.
- [22] Rim D, Novoselac A. Transient simulation of airflow and pollutant dispersion under mixing flow and buoyancy driven flow regimes in residential buildings. *ASHRAE Transactions* 2008;114(2):130–42.
- [23] FLUENT. Fluent 6.3 user's guide. Lebanon, NH: Fluent Inc.; 2006.
- [24] Posner JD, Buchanan CR, Dunn-Rankin D. Measurement and prediction of indoor air flow in a model room. *Energy and Buildings* 2003;35(5):515–26.
- [25] Etheridge D, Sandberg M. *Building ventilation: theory and measurement*. New York: Wiley; 1996.
- [26] Lai ACK, Nazaroff WW. Modeling indoor particle deposition from turbulent flow onto smooth surfaces. *Journal of Aerosol Science* 2000;31(4):463–76.

- [27] Lai ACK, Wang K, Chen FZ. Experimental and numerical study of particle distribution in a two-zone chamber. *Atmospheric Environment* 2008;42:1717–26.
- [28] Zhang A, Chen Q. Experimental measurements and numerical simulations of particle transport and distribution in ventilated rooms. *Atmospheric Environment* 2006;40:3396–408.
- [29] Sørensen DN, Neilsen PV. Quality control of computational fluid dynamics in indoor environments. *Indoor Air* 2003;13(1):2–17.
- [30] Waring M, Siegel J. Particle loading rates for HVAC filters, heat exchangers, and ducts. *Indoor Air* 2008;18(3):209–24.
- [31] Ferro AR, Kopperud RJ, Hildemann LM. Source strengths for indoor human activities that resuspend particulate matter. *Environmental Science and Technology* 2004;38(6):1759–64.
- [32] He CR, Morawska LD, Hitchins J, Gilbert D. Contribution from indoor sources to particle number and mass concentrations in residential houses. *Atmospheric Environment* 2004;38(21):3405–15.
- [33] Sun W, Ji J. Transport of droplets expelled by coughing in ventilated rooms. *Indoor and Built Environment* 2007;16(6):293–504.
- [34] Zhu SW, Kato S, Yang JH. Study on transport characteristics of saliva droplets produced by coughing in a calm indoor environment. *Building and Environment* 2006;41(12):1691–702.
- [35] Hinds WC. *Aerosol technology: properties, behavior, and measurement of airborne particles*. New York: Wiley; 1999.
- [36] ASHRAE. *ASHRAE standard 62.1 – ventilation for acceptable indoor air quality*. Atlanta, GA: American Society of Heating, Refrigerating and Air-Conditioning Engineers; 2006.
- [37] Zhao B, Wu J. Numerical investigation of particle diffusion in a clean room. *Indoor and Built Environment* 2005;14(6):469–79.
- [38] Wallace LA. Contribution of gas and electric stoves to residential ultrafine particle concentrations between 2 nm and 64 nm: Size distributions and emission and coagulation rates. *Environmental Science and Technology* 2008; 23:8641–6.